Regulation of embryonic neurogenesis by germinal zone vasculature

Mathew Tata[1], Ivan Wall[1,3], Andy Joyce[1], Joaquim M Vieira[1,4], Nicoletta Kessaris[2] and Christiana Ruhrberg[1,*]

[1] UCL Institute of Ophthalmology, University College London, 11-43 Bath Street, London EC1V 9EL, UK; [2] Wolfson Institute for Biomedical Research, University College London, Gower Street, London WC1E 6BT, UK

[3] current address: Department of Biochemical Engineering, University College London, Gordon Street, London,WC1E 6BT, UK

[4] current address: Department of Physiology, Anatomy and Genetics, University of Oxford, South Parks Road, Oxford OX1 3PT, UK

* author for correspondence:

Professor Christiana Ruhrberg
UCL Institute of Ophthalmology, University College London
11-43 Bath Street, London EC1V 9EL, UK
Tel.: +44 207 608 4017
Email: c.ruhrberg@ucl.ac.uk

Classification: Biological Sciences/Developmental Biology

Keywords: blood vessels, neural progenitor, neurogenesis, hindbrain, NRP1

Abstract

In the adult rodent brain, new neurons are born in two germinal regions that are associated with blood vessels, and blood vessels and vessel-derived factors are thought to regulate the activity of adult neural stem cells. Recently, it has been proposed that a vascular niche also regulates prenatal neurogenesis. Here, we identify the mouse embryo hindbrain as a powerful model to study embryonic neurogenesis and define the relationship between neural progenitor cell (NPC) behaviour and vessel growth. Using this model, we show that a subventricular vascular plexus (SVP) extends through a hindbrain germinal zone populated by NPCs whose peak mitotic activity follows a surge in SVP growth. Hindbrains genetically defective in SVP formation due to constitutive NRP1 loss showed a premature decline in both NPC activity and hindbrain growth downstream of precocious cell cycle exit, premature neuronal differentiation and abnormal mitosis patterns. Defective regulation of NPC activity was not observed in mice lacking NRP1 expression by NPCs, but in mice lacking NRP1 selectively in endothelial cells, yet was independent of vascular roles in hindbrain oxygenation. Germinal zone vascularisation therefore sustains NPC proliferation in the prenatal brain.

Significance statement

Neural progenitor cells (NPCs) proliferate to generate precursors for new neurons. To sustain this process, NPCs balance self-renewal with the generation of progeny committed to neuronal differentiation. In the adult mammalian brain, blood vessels and vessel-derived factors help to regulate this balance by modulating NPC proliferation and quiescence, independently of vascular roles in providing oxygen and nutrients. In contrast, vasculature has been proposed to regulate NPC behaviour in the developing forebrain by alleviating tissue hypoxia. We show here that germinal zone vasculature in the embryonic hindbrain regulates the balance of NPC self-renewal with neuron production, independently of roles in tissue oxygenation. Information on how blood vessels regulate neurogenesis may help design therapies for brain regeneration in injury and disease.

\body

Introduction

Stem cells are thought to reside within specialised niches that regulate their self-renewal and differentiation via signalling interactions; examples include notch signalling between osteoblasts and haematopoietic stem cells, extracellular matrix (ECM) signalling to epidermal stem cell integrins and paracrine WNT signalling across the intestinal crypt-villus axis (1). In the subventricular zone of the lateral ventricles (LV/SVZ) in the adult rodent brain, neural stem cells (NSCs) reside in a specialised niche composed of ependymal cells at the ventricle wall and peri-germinal blood vessels (2). LV/SVZ endothelium expresses notch, ephrins and the neurotrophins PEDF and NT3 to maintain quiescence and pluripotency of the NSCs (3-5), and losing close contact with LV/SVZ vessels therefore increases NSC proliferation (6). Moreover, cultured LV/SVZ-derived NSC use integrins to attach to laminin-expressing vessels to regulate their mitotic activity (7). The vascular endothelial growth factors VEGF-A and VEGF-C also contribute to NSC regulation, with the former suggested to promote NSC proliferation through VEGFR2 (8), and the latter enhancing neuron production from NSCs through VEGFR3 in the LV/SVZ and hippocampal neurogenic niches (8, 9).

These studies indicate important roles for vascular growth factors, blood vessels and vessel-derived factors in regulating NSC behaviour in the adult mammalian brain. In contrast, it is poorly understood how VEGF or blood vessels regulate neurogenesis in the embryonic brain. This is a fundamental question, because despite many similarities, adult and embryonic neurogenesis differ in several respects. Most notably, embryonic neurogenesis arises from an abundant pool of neural progenitor cells (NPCs), which initially proliferate rapidly and then progressively lose their proliferative capacity as they generate a large number of neural progeny with great functional diversity. Moreover, developmental neurogenesis leads to rapid brain growth that necessitates extensive expansion of supporting vasculature, whereas vascular growth is scarce and NSCs proliferate slowly in the adult brain. A recent study suggested that blood vessels alleviate tissue hypoxia in the embryonic dorsal forebrain to promote the commitment of self-renewing NPCs to fate-restricted progenitors (10). Another study suggested that vessels in the ventral forebrain provide anchorage for NPCs that give rise to cortical interneurons (11). However, whether blood vessels regulate neurogenesis in other regions of the central nervous system (CNS) is unknown.

Neuropilin 1 (NRP1) is a cell surface receptor that is expressed by blood vessels and NPCs in the embryonic CNS (12, 13). NRP1 promotes CNS vascularisation in response to VEGF-A and ECM signals (14, 15) and functions as a VEGF-A and class 3 semaphorin (SEMA3) receptor to regulate neuronal migration and axon guidance (16). Moreover, SEMA3B signals through NRP1 and NRP2 in spinal cord NPCs to orientate their mitotic spindle and regulate the onset of motor neuron differentiation (13). However, it has not yet been examined whether NRP1 acts as a VEGF-A receptor in NPCs, nor is it known whether NRP1-dependent vasculature regulates NPC behaviour. Here, we show that NRP1 ablation in the mouse embryo hindbrain caused precocious NPC cell cycle exit and therefore premature neural differentiation. This defect was phenocopied in mice lacking NRP1 in endothelial cells, but not the NPC lineage, demonstrating an important role for NRP1-dependent germinal zone (GZ) vasculature, rather than VEGF-A signalling through NRP1 in NPCs, in regulating hindbrain neurogenesis. We further found that vasculature regulated NPC self-renewal independently of its role in alleviating tissue hypoxia. Moreover, hindbrains lacking GZ vasculature showed abnormal patterns of NPC mitoses. These findings identify the mouse embryo hindbrain as a powerful model to study the anatomical and functional relationship of

vessel growth and neurogenesis and demonstrate that hindbrain neurogenesis is sustained by a NRP1-dependent vascular niche.

Results

Hindbrain NPCs proliferate rapidly after a peak in vessel sprouting

We studied the spatiotemporal relationship of NPC proliferation and CNS vascularisation in the developing hindbrain, as its flat architecture is exquisitely suited to visualising growing vessels near the ventricular surface and NPC mitosis in the ventricular zone (VZ). Thus, wholemount staining of embryonic day (e) 11.5 hindbrains, corresponding to the 45 somite pair (s) stage (**Table S1**), identified an isolectin B4 $(IB4)^+$ subventricular vascular plexus (SVP) (12) beneath a layer of phosphohistone H3 $(pHH3)^+$ cells corresponding to mitotic NPCs (**Fig. 1A,B**). 3-dimensional surface rendering demonstrated that filopodia extended from the SVP towards the VZ in gaps between NPCs (**Fig. 1B'**). Hindbrain NPCs therefore proliferate near GZ vasculature. To compare the progression of GZ vascularisation and NPC proliferation over time, we performed wholemount IB4 staining of wildtype hindbrains from mice on a CD1 genetic background. We observed that only a few vessel sprouts had entered the e9.5/25s hindbrain, but vessel sprouting peaked beneath the VZ at e10.5/35s (**Fig. 1C,D**). Vessel sprouting declined from e11.5/45s onwards (**Fig. 1C,D**), when vessel sprouts anastomose to form the SVP (12). Wholemount $pHH3^+$ staining showed that NPC mitotic activity spanned the period from e9.5/25s to e12.5/50s (**Fig. 1E**) and therefore correlated with the major phase of hindbrain angiogenesis. The peak in NPC mitoses occurred around e11.0/40s, shortly after the peak in vessel sprouting, but declined again after the SVP was established (**Fig. 1E,F**). A small proportion of $pHH3^+$ cells displayed weaker pHH3 staining and formed crescent-shaped pairs (far-right panel in **Fig. 1E**), typical for cells transitioning from anaphase to early telophase (17). These cells are hereafter referred to as anaphase NPCs and typically comprised 20±6.5% of the total mitotic population. The time course of NPC proliferation was similar in C57BL/6 mice, but occurred slightly earlier than in CD1 mice and with a peak that was less pronounced (**Fig. 1F**). Together, these experiments show that vessel sprouting correlates with a surge in NPC mitosis. The hindbrain is therefore a suitable model to study the relationship of NPC proliferation and GZ vasculature in the developing brain.

Spatial relationship between hindbrain NPCs and vasculature

To define the spatial relationship of mouse hindbrain NPCs with GZ vasculature, we examined transverse sections of hindbrains from the avascular stage to the time when VZ mitotic activity had largely subsided. In contrast to the forebrain, where mitotic NPCs are distributed both at the ventricular surface and in the subventricular zone, mitotic NPCs in the hindbrain were largely confined to a single layer adjacent to the ventricular wall (**Fig. 2A**). Beneath this layer of mitotic NPCs, BrdU-labelled S-phase NPC nuclei adopted a pseudostratified organisation (**Fig. 2A**), suggesting that hindbrain NPCs undergo interkinetic nuclear migration (INM), similar to telencephalic NPCs (18). At e9.5/25s, a small number of radial vessels had invaded the hindbrain from the perineural vascular plexus (PNP) (**Fig. 2A**). At e10.5/35s, radial vessels had sprouted perpendicularly to initiate SVP formation at an average depth of 21.8±1.5 μm from the ventricular surface (**Fig. 2A**). The emerging SVP passed directly through the GZ, and from around e10.5/35s onwards, the S-phase NPC nuclei appeared to gather around the SVP (**Fig. 2A**). From e11.5/45s, a deep vessel plexus (DP) formed underneath the GZ (**Fig. 2A**). Hindbrain vasculature therefore has a clear anatomical relationship with proliferating NPCs.

Hindbrain NPCs contact the SVP and vessel-associated ECM

The RC2 antibody for the intermediate filament protein nestin visualises NPC processes in the developing brain (19). RC2 staining was sparse in the hindbrain ventricular region at e9.5/25s, but appeared stronger towards the pial surface (**Figs. 2B** and **S1A**). At e10.5/35s, $RC2^+$ processes extended from the apical towards the pial surface (**Figs. 2C** and **S1A**). $RC2^+$ endfeet appeared to project onto the laminin-rich basement membrane adjacent to the PNP from e9.5/25s (**Fig. 2B**). Higher magnification showed close apposition of a subset of $RC2^+$ fibres with laminin-coated SVP vessels (**Figs. 2C** and **S1A'**). At e12.5/50s, towards the end of the neurogenesis period, $RC2^+$ processes were denser in the apical hindbrain (**Fig. S1A**). To visualise the interaction of $RC2^+$ processes from individual NPCs with blood vessels, we performed mosaic labelling with a tamoxifen-inducible *Sox1-iCreER*^{T2} transgene and the recombination reporter *Rosa*$^{tdTomato/+}$ (see supplemental methods). CRE-mediated recombination was detected by immunostaining for the Tomato protein in a subset of NPCs at 35s (**Fig. S1B**). 3-dimensional surface rendering of confocal z stacks established that some NPC processes wrapped tightly around GZ vessels (**Fig. 3A,B,D**), whilst others terminated with endfeet on the PNP (**Fig. 3A,C**). NPCs therefore physically interact with hindbrain vessels.

NRP1 regulates the temporal pattern of hindbrain NPC mitoses

NRP1 is expressed by hindbrain endothelium and NPCs (12), is essential for hindbrain vascularisation (20) and cooperates with NRP2 to regulate SEMA3B-mediated NPC division plane orientation in the spinal cord (13). To determine how NRP1 loss affects GZ vascularisation and neurogenesis, we compared stage-matched *Nrp1*-null mutant and control hindbrains (stage matching was performed to account for a developmental delay caused by NRP1 loss; **Table S1** and **Fig. S2**). Consistent with prior findings (20), radial vessels had entered 32s *Nrp1*-null hindbrains, but failed to branch laterally to form the SVP (**Fig. 4A**). In 40s mutants, occasional vessels had entered the GZ, but formed abnormal vascular tufts; other vessels branched laterally beneath the GZ, forming a deep plexus of abnormally large calibre (**Fig. 4A**). Quantification confirmed that the GZ was largely avascular in mutants (**Fig. 4B**). Despite the lack of GZ vasculature, apoptosis was not increased in 32s or 40s *Nrp1*-null hindbrains compared to controls (**Fig. S3**). Thus, the rudimentary network of radial and deep plexus vessels, combined with an intact PNP and a flat hindbrain architecture, was likely sufficient to maintain hindbrain health during neurogenesis.

GZ organisation into a ventricular mitotic NPC layer and a pseudostratified layer of $BrdU^+$ NPC S-phase nuclei was maintained in the mutants (**Fig. 4A**). Moreover, NPC processes in *Nrp1*-null hindbrains extended between the ventricular and pial hindbrain surfaces, suggesting that anchorage to pial ECM was not perturbed; however, there was mild disorganisation of NPC processes in some regions lacking vessels (**Fig. S4**). Furthermore, the GZ of mutant hindbrains appeared thicker at 32s, but thinner at 40s than in controls (**Fig. 4A,C**). Wholemount imaging of $pHH3^+$ NPCs in the VZ between the 32s and 46s stages suggested an abnormal time course of NPC proliferation in *Nrp1*-null hindbrains, with a premature increase and subsequent decline of mitotic NPC numbers (**Fig. 4D,E**). Quantification of the number of $pHH3^+$ cells in a detailed time course between 25s and 46s demonstrated that the number of mitotic NPCs was still similar in mutant and control VZ at the 25s stage, when the hindbrain is still largely avascular (**Fig. 4E**). In contrast, the number of $pHH3^+$ NPC figures in the VZ of mutants had increased slightly at 32s and prominently at 36s (**Fig. 4D,E**). Surprisingly, the large increase in the overall number of $pHH3^+$ NPCs in mutants at 36s could be attributed to a transient and striking increase in the number of NPCs in

anaphase (**Fig. 4D,E** and **Fig. S5**), because the number of pHH3$^+$ pre-anaphase NPCs was similar between wildtype and *Nrp1*-null mutant hindbrains (all pHH3$^+$ mitotic figures minus pHH3$^+$ anaphase figures; **Fig. S5**). This finding suggests mitotic stalling in the mutant hindbrain at 36s. The proportion of anaphases was again similar in mutants and controls at 40s and 42s, but this apparent normalisation was transient as the anaphase phenotype inverted, with the proportion of NPCs in anaphase lower in mutant than control VZ at the 46s stage (**Fig. 4D,E**). At the 46s stage, when NPC activity begins to subside in wildtype hindbrains, the overall number of mitotic NPCs was even lower in mutants than controls, indicated by a significantly reduced number of pHH3$^+$ cells in VZ flatmounts (**Fig. 4D,E**) that was confirmed in subsequent analyses by a reduced number of Ki67$^+$ NPCs in *Nrp1*$^{-/-}$ embryos (see below). NRP1 is therefore required for a normal pattern of NPC proliferation in the hindbrain and to sustain NPC activity.

NRP1 regulates NPC division through its role in vessel growth

To distinguish whether NRP1-dependent blood vessels or NRP1 signalling in NPCs regulate hindbrain neurogenesis, we analysed *Tie2-Cre*;*Nrp1*$^{c/-}$ and *Nes-Cre*;*Nrp1*$^{c/-}$ mutant mice, which were previously shown to lack NRP1 in the endothelial or neural lineage, respectively (20). *Nes-Cre*;*Nrp1*$^{c/-}$ mutants have normal hindbrain vascularisation; in contrast, *Tie2-Cre*;*Nrp1*$^{c/-}$ mutants have vascular defects similar to, but milder than those of full NRP1 knockouts, due to the persistence of a few recombination-resistant endothelial cells that enable low level vessel sprouting (20). We found that *Tie2-Cre*;*Nrp1*$^{c/-}$ mutants had an avascular GZ at 32s, but GZ vascularisation had partially recovered at 48s (**Fig. S6A**). As observed in constitutive *Nrp1*-null mutants, NPC processes extended between the ventricular and pial surfaces in *Tie2-Cre*;*Nrp1*$^{c/-}$ hindbrains, but there was mild disorganisation of NPC processes in some regions lacking vessels (**Fig. S6B**).

Quantification demonstrated that *Tie2-Cre*;*Nrp1*$^{c/-}$ mutant VZ had an abnormal pattern of pHH3$^+$ NPC mitoses, including a greater proportion of anaphase NPCs than control VZ at 36s and significantly less NPC mitosis thereafter (**Figs. 4F,G**). Thus, endothelial *Nrp1*-null mutants have a NPC mitosis defect similar to constitutive *Nrp1*-null mutants. However, the defect was milder in endothelial compared to full NRP1-null mutants (compare **Fig. 4G** with **Fig. 4E**), correlating with a milder defect in GZ vascularisation (compare **Fig. S6A** with **Fig. 4A**). In contrast, *Nes-Cre*;*Nrp1*$^{c/-}$ mutant hindbrains had a similar number of NPC mitoses compared to controls at all stages examined (**Figs. 4F,H**; somite counting excluded a developmental delay in *Nes-Cre*;*Nrp1*$^{c/-}$ mutants). As VEGFR2 (FLK) is an alternative VEGF-A receptor expressed in NPCs derived from embryonic telencephalon (21), we asked whether it might compensate for NRP1 in hindbrain NPCs. However, NPCs did not obviously express VEGFR2 (**Fig. S7**). The lack of VEGFR2 expression in hindbrain NPCs, together with a normal number of NPC mitoses in *Nes-Cre;Nrp1*$^{c/-}$ mutants, suggests that VEGF-A is unlikely to directly regulate NPC proliferation during hindbrain neurogenesis. Instead, NRP1-dependent GZ vasculature regulates hindbrain neurogenesis.

Hindbrain vasculature promotes NPC self-renewal independently of tissue oxygenation

Whereas pHH3 staining had suggested cell cycle stalling in mitosis at the 36s stage when GZ vessel sprouting peaks, NPC mitotic behaviour was only subtly affected at 32s, when blood vessels first enter the GZ to form the SVP (**Fig. 4**). We therefore performed additional experiments at 32s to examine whether GZ vascularisation helps to sustain the proliferative capacity of NPCs. Thus, we injected pregnant dams with BrdU 24 h before isolating 32s hindbrains and then immunolabelled with antibodies for BrdU and the proliferation marker Ki67 (**Fig. 5A**). NPCs that had undergone terminal divisions after the BrdU injection would be labelled with BrdU only, whereas self-

renewing NPCs, i.e. cells that continued to cycle, would be double positive for BrdU and Ki67 (22). Strikingly, 25% fewer NPCs were double positive in *Nrp1*-null than control hindbrains (**Fig. 5B,C**). This decrease in cycling NPCs inversely correlated with a larger area labelled with TUJ1, a marker for postmitotic neurons (**Fig. 5B,C**). Therefore, an increased proportion of NPCs undergoes cell cycle exit at 32s. Moreover, this analysis demonstrated ectopic neuronal differentiation in the VZ of mutants (**Fig. 5B**). Similar, but milder defects in NPC self-renewal were observed in embryos selectively lacking endothelial NRP1 (**Fig. 5B,C**). Accordingly, a substantial proportion of NPCs undergoes precocious and incorrectly placed neurogenesis in hindbrains failing to establish GZ vasculature due to NRP1 deficiency.

Interestingly, even though the absolute number of $Ki67^+$ cycling NPCs had significantly decreased by 46s (**Fig. S8A**), the relative proportion of $Ki67^+$ cycling NPCs in all $BrdU^+$ NPCs was similar in *Nrp1*-null mutant and control hindbrains at this stage (**Fig. S8B**). However, regaining this equilibrium between cycling and differentiating NPCs at this late stage in the neurogenesis time course had failed to avert the overall loss of NPC proliferative capacity for hindbrain growth, because hindbrain depth along the apicobasal axis and cross-sectional hindbrain area were significantly reduced at 46s in mutants compared to controls (**Fig. S8C,D**). Taken together, these observations suggest that the NPC pool was prematurely depleted in hindbrains lacking GZ vasculature, with severe consequences for hindbrain growth.

We examined whether increased tissue hypoxia due to vascular insufficiency was responsible for these neurogenesis defects. Thus, premature cell cycle exit occurred at a time when the hindbrain was less oxygenated in *Nrp1*-null mutants compared to controls, demonstrated by increased expression of the hypoxia-induced genes *Hif1a* and *Vegfa* and higher protein levels of the hypoxia-responsive glucose transporter GLUT1 (**Fig. S9A,C,D**). Housing pregnant dams in an 80% oxygen atmosphere for 24 h prior to embryo collection (10) restored hindbrain oxygenation, but failed to rescue the self-renewal and neuronal differentiation defects in NRP1-null hindbrains (**Fig. S9B-D**). Therefore, GZ vasculature regulates hindbrain neurogenesis independently of its role in tissue oxygenation.

Discussion

Here, we have identified the mouse embryo hindbrain as a powerful model to study neurogenesis with unique advantages. These include the ability to capture the extent and prevalence of organ-wide NPC mitoses in flatmounted VZ for quantitative analysis and to study a proliferating neuroepithelium in which most NPC mitoses are confined to a region immediately adjacent to the ventricular surface. Moreover, we were able to take advantage of established genetic mouse models to distinguish the possibility that NRP1 acts in hindbrain NPCs as a receptor for ligands such as VEGF-A from an indirect role in regulating hindbrain neurogenesis through its role in blood vessel patterning. We found that NRP1 expression by endothelial cells, but not NPCs, was required to regulate NPC mitotic behaviour (**Fig. 4**). Prior *in vitro* studies showed that NPCs in neurospheres derived from e14 forebrain express VEGFR2, and that exogenous VEGF-A increased neurosphere number and cell survival (21). However, another forebrain study found that VEGFR2 is endogenously expressed in the endothelial cells of the embryonic brain, but not in non-endothelial cells such as NPCs (23). In agreement with the latter study, we did not detect obvious VEGFR2 expression in the hindbrain VZ (**Fig. S7**). It therefore appears unlikely that NRP1 or VEGFR2 convey VEGF-A signals to regulate hindbrain NPC proliferation. We have not investigated whether

NRP1 in hindbrain NPCs cooperates with NRP2 to convey semaphorin signals for mitotic spindle orientation, as reported for the spinal cord (13), because the NPC defect we describe here could be attributed to defective NRP1 signalling in endothelial cells, rather than cell autonomous NRP1 signalling in NPCs (**Fig. 4**). Thus, our findings in the mouse embryo hindbrain agree with those in the adult brain, which showed that vasculature sustains NSC proliferation (3-5, 24).

Hindbrain NPC mitosis normally peaks at the time when angiogenic sprouting is maximal in the GZ and begins to subside once sprouts fuse into the SVP that provides the GZ vasculature (**Figs. 1** and **2**). Agreeing with a functional role of GZ vasculature in regulating hindbrain neurogenesis, we observed that a considerable proportion of hindbrain NPCs underwent premature cell cycle exit in both constitutive and endothelial-specific *Nrp1*-null mutants lacking GZ vasculature (**Fig. 5**). Subsequently, a proportion of those NPCs that had not exited the cell cycle by the 32s stage showed abnormal mitotic NPC behaviour in both constitutive and endothelial-specific *Nrp1*-null mutants lacking GZ vasculature. In particular, the proportion of NPCs in anaphase amongst all mitotic NPCs was increased in these mutants at a time when GZ vasculature is normally established, but was lacking in mutants (**Fig. 4** and **S5**). Prolonged mitosis has been reported to skew the fate of dividing NPCs towards the generation of neurons at the expense of generating further NPCs (25). With combined defects in excessive NPC cell cycle exit at 32s and mitotic NPC stalling at 36s in *Nrp1* mutants lacking GZ vasculature, it was therefore not surprising that the pool of cycling progenitors was considerably depleted by the 46s stage, when hindbrain growth was accordingly severely compromised (**Fig. S8**).

We cannot currently explain why some NPCs in *Nrp1* mutant hindbrains undergo precocious cell cycle exit at 32s, whilst others continue to cycle beyond the 32s stage only to stall in anaphase; nor do we know why anaphase stalling at 36s reverses into accelerated anaphase transition at 46s in *Nrp1* mutants lacking GZ vasculature. One possibility why loss of GZ vasculature may differently affect NPC behaviour at successive developmental stages may be that specific NPC subsets change their responsiveness to multiple, overlapping extrinsic signals over time. In analogy, it has been observed that sonic hedgehog signals increase S-phase length in spinal motor neuron progenitors as brain development progresses, with a prolonged S-phase and therefore longer cell cycle time in self-renewing NPCs in younger embryos (26). Alternatively, distinct subsets of NPCs, generated in consecutive phases and acting as progenitors for different neural or glial subtypes, may respond differently to vessel-derived cues, as reported for interneuron-committed NPCs in the ventral forebrain (11). Importantly, our observations suggest that the hindbrain model is exquisitely suited to identify how extrinsic factors regulate the behaviour of changing NPC populations over time.

The anatomical relationship of NPCs and GZ vasculature in the hindbrain is reminiscent of that recently described for the forebrain, where NPCs and their processes also cluster around vessels (23, 27). Moreover, loss of GZ vasculature increased hypoxia in the hindbrain (**Fig. S9**), as was recently reported for the forebrain (10). Interestingly, tissue hypoxia in the dorsal forebrain impaired NPC commitment towards neural specification (10). In contrast to the forebrain, however, we observed increased NPC commitment and neuronal differentiation in hindbrains lacking GZ vasculature (**Fig. 5**). Moreover, a hypoxic insult was not the obvious cause of the observed hindbrain NPC defect, because NPC self-renewal and premature neuronal differentiation were not rescued by restoration of tissue oxygenation (**Fig. S9**). The *Nrp1*-null mutant hindbrain therefore provides a mammalian model suited to determine the role of GZ vasculature in neurogenesis independently of the general role of blood vessels in maintaining tissue oxygenation. The different

requirements for blood vessels identified in the prior forebrain study and our current work on hindbrain neurogenesis may reflect differences in the NPC subtypes present in both organs; thus, $TBR2^+$ basal progenitors are abundant in the forebrain, but are not found in the hindbrain (28). Alternatively, or additionally, the different neurogenesis defects observed in the forebrain and hindbrain studies may be explained by the use of different mouse models. In particular, NRP1-deficient hindbrains specifically lack GZ vasculature, but contain patent vasculature in other hindbrain areas (**Fig. 4**) (20), whereas forebrain vasculature in GPR124 mutants is severely haemorrhagic and therefore likely leaky and poorly functional (29). Moreover, a low level of apoptosis in the *Nrp1*-deficient hindbrain (**Fig. S3**) may be explained, in part, by the hindbrain's uniquely flat architecture, which instils proximity of tissue components to the PNP and cerebrospinal fluid for nourishment.

In summary, we have shown here that hindbrain GZ vasculature provides essential extrinsic signals above and beyond its role in tissue oxygenation to modulate the NPC cell cycle and therefore sustain neurogenesis. Taken together with the recent forebrain studies identifying oxygen-dependent regulation of NPC commitment, GZ vasculature is therefore a crucial component of the embryonic niche for neurogenesis, with region-specific roles in regulating NPC fate and the onset of neuronal differentiation. It is not presently clear whether the previously discovered functions of blood vessels in paracrine or contact-dependent modulation of adult NSCs also operate in the embryonic hindbrain NPC niche. The observations that angiogenesis and neurogenesis proceed in overlapping spatiotemporal windows (**Figs. 1** and **2**) and that hindbrain (**Fig. 3**) and ventral forebrain (11) NPC processes seemingly wrap around GZ vessels are certainly consistent with both possibilities. Importantly, however, it cannot be assumed that specific molecules operating in the adult neurogenic niche have similar roles in the embryo. Accordingly, differences in the extrinsic regulation of adult and embryonic neurogenesis are plentiful (30), as exemplified by opposing roles of niche-derived signals such as NT3 in mediating quiescence of adult NSC (4) versus commitment of embryonic NPCs to neuronal differentiation (31). Future work might therefore exploit the unique advantages of the hindbrain model to organ-wide imaging and quantitative analysis to identify the signalling mechanisms that underlie the vascular regulation of NPC maintenance and differentiation in the developing mammalian brain.

Materials and Methods

Animal work was carried out following UK Home Office and local ethical guidelines. *Nrp1*-null CD1 mice and endothelial- or NPC-specific NRP1-null C57/Bl6 mice have been described (15, 20). *Sox1-iCreER*^{T2} mice were developed by N.K. and crossed to *Rosa*^{tdTomato} reporter mice (32). To obtain embryos of defined developmental stages, mice were paired overnight and the day of finding a copulation plug was designated embryonic day (e) 0.5. In some experiments, pregnant females were injected intraperitoneally with 10 mg/kg BrdU. Dissected hindbrains were immunostained as described previously (33) and the number of proliferating NPCs quantified by manual counting. To determine whether two datasets were significantly different, we used a two-tailed, unpaired *t* test. For further detail, see SI Materials and Methods.

Author contributions

MT, IW, JV and CR designed the research, MT, IW, NK and AJ performed the research, MT and CR analysed the data and wrote the manuscript.

Acknowledgements

We thank U Dennehy, M Daglish, A Fantin, L Denti, as well as the Biological Resources Unit and Imaging Facility of the UCL Institute of Ophthalmology for technical help. We thank WD Richardson for contributions to generating *Sox1-iCreER^{T2}* mice and M Golding, F Guillemot and F Doetsch for valuable advice. This study was supported by a Wellcome Trust PhD studentship to MT [096621/Z/11/Z] and an Investigator Award to CR [095623/Z/11/Z], Medical Research Council grants to CR [G0601093], WD Richardson and NK [G0800575] and a European Research Council Starting Grant to NK [207807].

References

1. Li L & Xie T (2005) Stem cell niche: structure and function. *Annu Rev Cell Dev Biol* 21:605-631.
2. Tavazoie M, *et al*. (2008) A specialized vascular niche for adult neural stem cells. *Cell Stem Cell* 3(3):279-288.
3. Ottone C, *et al*. (2014) Direct cell-cell contact with the vascular niche maintains quiescent neural stem cells. *Nat Cell Biol* 16(11):1045-1056.
4. Delgado AC, *et al*. (2014) Endothelial NT-3 delivered by vasculature and CSF promotes quiescence of subependymal neural stem cells through nitric oxide induction. *Neuron* 83(3):572-585.
5. Andreu-Agullo C, Morante-Redolat JM, Delgado AC, & Farinas I (2009) Vascular niche factor PEDF modulates Notch-dependent stemness in the adult subependymal zone. *Nat Neurosci* 12(12):1514-1523.
6. Niola F, *et al*. (2012) Id proteins synchronize stemness and anchorage to the niche of neural stem cells. *Nat Cell Biol* 14(5):477-487.
7. Shen Q, *et al*. (2008) Adult SVZ stem cells lie in a vascular niche: a quantitative analysis of niche cell-cell interactions. *Cell Stem Cell* 3(3):289-300.
8. Jin K, *et al*. (2002) Vascular endothelial growth factor (VEGF) stimulates neurogenesis in vitro and in vivo. *Proc Natl Acad Sci U S A* 99(18):11946-11950.
9. Calvo CF, *et al*. (2011) Vascular endothelial growth factor receptor 3 directly regulates murine neurogenesis. *Genes Dev* 25(8):831-844.
10. Lange C, *et al*. (2016) Relief of hypoxia by angiogenesis promotes neural stem cell differentiation by targeting glycolysis. *EMBO J* 35(9):924-941.
11. Tan X, *et al*. (2016) Vascular Influence on Ventral Telencephalic Progenitors and Neocortical Interneuron Production. *Dev Cell* 36(6):624-638.
12. Fantin A, *et al*. (2010) Tissue macrophages act as cellular chaperones for vascular anastomosis downstream of VEGF-mediated endothelial tip cell induction. *Blood* 116(5):829-840.
13. Arbeille E, *et al*. (2015) Cerebrospinal fluid-derived Semaphorin3B orients neuroepithelial cell divisions in the apicobasal axis. *Nat Commun* 6:6366.
14. Raimondi C, *et al*. (2014) Imatinib inhibits VEGF-independent angiogenesis by targeting neuropilin 1-dependent ABL1 activation in endothelial cells. *The Journal of Experimental Medicine* 211(6):1167-1183.
15. Fantin A, *et al*. (2015) NRP1 Regulates CDC42 Activation to Promote Filopodia Formation in Endothelial Tip Cells. *Cell Rep* 11(10):1577-1590.
16. Mackenzie F & Ruhrberg C (2012) Diverse roles for VEGF-A in the nervous system. *Development* 139(8):1371-1380.
17. Hans F & Dimitrov S (2001) Histone H3 phosphorylation and cell division. *Oncogene* 20(24):3021-3027.
18. Sauer F (1935) Mitosis in the neural tube. *Journal of Comparative Neurology* 62(2):377-405.
19. Haubst N, *et al*. (2006) Basement membrane attachment is dispensable for radial glial cell fate and for proliferation, but affects positioning of neuronal subtypes. *Development*

133(16):3245-3254.
20. Fantin A, *et al*. (2013) NRP1 acts cell autonomously in endothelium to promote tip cell function during sprouting angiogenesis. *Blood* 121(12):2352-2362.
21. Wada T, *et al*. (2006) Vascular endothelial growth factor directly inhibits primitive neural stem cell survival but promotes definitive neural stem cell survival. *J Neurosci* 26(25):6803-6812.
22. Arnold SJ, *et al*. (2008) The T-box transcription factor Eomes/Tbr2 regulates neurogenesis in the cortical subventricular zone. *Genes Dev* 22(18):2479-2484.
23. Javaherian A & Kriegstein A (2009) A stem cell niche for intermediate progenitor cells of the embryonic cortex. *Cereb Cortex* 19 Suppl 1:i70-77.
24. Crouch EE, Liu C, Silva-Vargas V, & Doetsch F (2015) Regional and stage-specific effects of prospectively purified vascular cells on the adult V-SVZ neural stem cell lineage. *J Neurosci* 35(11):4528-4539.
25. Pilaz LJ, *et al*. (2016) Prolonged Mitosis of Neural Progenitors Alters Cell Fate in the Developing Brain. *Neuron* 89(1):83-99.
26. Saade M, *et al*. (2013) Sonic hedgehog signaling switches the mode of division in the developing nervous system. *Cell Rep* 4(3):492-503.
27. Stubbs D, *et al*. (2009) Neurovascular congruence during cerebral cortical development. *Cereb Cortex* 19 Suppl 1:i32-41.
28. Kwon GS & Hadjantonakis AK (2007) Eomes::GFP-a tool for live imaging cells of the trophoblast, primitive streak, and telencephalon in the mouse embryo. *Genesis* 45(4):208-217.
29. Kuhnert F, *et al*. (2010) Essential regulation of CNS angiogenesis by the orphan G protein-coupled receptor GPR124. *Science* 330(6006):985-989.
30. Urban N & Guillemot F (2014) Neurogenesis in the embryonic and adult brain: same regulators, different roles. *Front Cell Neurosci* 8:396.
31. Parthasarathy S, *et al*. (2014) Ntf3 acts downstream of Sip1 in cortical postmitotic neurons to control progenitor cell fate through feedback signaling. *Development* 141(17):3324-3330.
32. Madisen L, *et al*. (2010) A robust and high-throughput Cre reporting and characterization system for the whole mouse brain. *Nat Neurosci* 13(1):133-140.
33. Fantin A, *et al*. (2013) The embryonic mouse hindbrain as a qualitative and quantitative model for studying the molecular and cellular mechanisms of angiogenesis. *Nat Protoc* 8(2):418-429.

Figure legends

Figure 1: Temporal correlation of blood vessel growth and NPC proliferation in the hindbrain. (**A**) Schematic representation of a flatmounted e11.5 hindbrain containing mitotic NPCs (green) and blood vessels (red). The blue box indicates the area imaged in (**B,C,E**), the eye illustrates the observer's point of view. (**B,B'**) Proximity of SVP vessels to mitotic NPCs. Maximal projection (xy) of a confocal z stack (**B**) through flatmounted e11.5 hindbrains after labelling with the dual vessel and microglia marker IB4 (red) and the mitotic marker pHH3 (green). Scale bar: 100 μm. 3D surface rendering (**B'**) illustrates the SVP beneath a layer of mitotic NPCs. The higher magnification of the boxed area shows endothelial cell filopodia projecting between the mitotic NPCs towards the ventricular surface. (**C-F**) Time course of vessel sprouting and NPC proliferation in the hindbrain. Maximal projection (xy) of confocal z stacks through flatmounted hindbrains at the indicated stages after IB4 labelling, including quantification of vessel sprouts (**C,D**) and mitotic and anaphase NPCs in CD1 and C57BL6 backgrounds after pHH3 labelling (**E,F**). Scale bar: 100μm. In (**C**), examples of vessel sprouts and microglia are indicated with arrowheads and open arrowheads, respectively. The boxed area in (**E**) is shown at higher

magnification to illustrate strongly labelled metaphase NPCs (wavy arrow) and dimly labelled anaphase NPCs (arrow). Data are shown as mean ± standard deviation of the mean; n≥3 for each time point.

Figure 2: Spatial relationship of blood vessel growth and NPC proliferation in the hindbrain. Confocal z stacks of 70 μm transverse sections of wildtype hindbrains at the indicated stages after labelling with IB4 together with antibodies for pHH3 and BrdU (**A**) or RC2 and LAMA1 (**B,C**). Scale bar: 20 μm. The boxed areas in (**B,C**) are shown in higher magnification adjacent to each panel (**B',C'**). Single (1.25 μm) optical sections from these projections are displayed underneath (**B'',C''**). Arrowheads in (**B,C**) indicate IgM^+ blood cells labelled with the secondary antibody used for RC2 detection. The wavy arrow in (**B''**) indicates NPC endfeet. Arrows and curved arrow in (**C**) denote NPC processes and density near SVP vessels. Abbreviations: P, pial surface; V, ventricular surface; RV, radial vessel; DP, deep plexus.

Figure 3: Hindbrain NPC processes contact the SVP. 3D surface rendering of confocal z stacks of *Sox1-iCreER^{T2};Rosa^{tdTomato}* hindbrain sections after labelling for RFP (red) together with IB4 (green). Boxed areas in (**A**) are shown in higher magnification in (**B-D**). Arrows denote NPC processes, wavy arrows NPC endfeet and the curved arrow an NPC density near blood vessels. Scale bar: 50μm.

Figure 4: NRP1 regulates hindbrain GZ vascularisation and NPC proliferation. (**A-C**) *Nrp1*-null mutants lack GZ vasculature. Maximal projections (xy) of confocal z stacks from hindbrain sections at the indicated stages after labelling for pHH3 and BrdU together with IB4 (**A**). Brackets denote GZ depth, the arrowhead a dead-ended radial vessel and the straight arrow an abnormal deep plexus. Scale bar: 100 μm. Abbreviations: P, pial surface; V, ventricular surface; DP, deep plexus. (**B,C**) Quantification of GZ vascular coverage as $IB4^+$ per $BrdU^+$ GZ area (**B**) and GZ thickness as average depth of the $BrdU^+$ GZ area (**C**). (**D-H**) Abnormal NPC proliferation in *Nrp1* mutants. Maximal projection (xy) of confocal z stacks of flatmounted wildtype versus *Nrp1*-null (**D**) and *Nrp1$^{c/+}$* control versus *Tie2-Cre;Nrp1$^{c/-}$* or *Nes-Cre;Nrp1$^{c/-}$* (**F**) hindbrain VZ at the indicated stages after pHH3 labelling. Quantification of $pHH3^+$ NPCs in the VZ, including proportion of NPCs in anaphase, per 0.25 mm^2 VZ at the indicated stages for constitutive (**E**) or cell type selective (**G,H**) *Nrp1*-null and stage-matched control hindbrains. In (**E**), red and blue arrows indicate the onset of SVP formation and peak vessel sprouting in wildtype hindbrains, respectively. All graphs show the mean ± standard deviation of the mean, n≥3 for each time point and genotype; * $p<0.05$, ** $p<0.01$, *** $p<0.001$.

Figure 5: Premature neurogenesis in constitutive and endothelial *Nrp1*-null hindbrains.

(**A**) Schematic representation of BrdU labelling. Embryos received BrdU on e9.5 and were analysed on e10.5. The blue line represents the pattern of NPC mitosis during hindbrain neurogenesis.

(**B**) 10 μm transverse sections from 32s hindbrains of the indicated genotypes were labelled for BrdU and Ki67 or with TUJ1 and the nuclear counterstain DAPI. Scale bar: 20μm. Dotted lines demarcate the basal hindbrain surface. Arrowheads indicate examples of $Ki67^-/BrdU^+$ cells; arrows denote ectopic TUJ1 staining in the VZ. Abbreviations: P, pial surface; V, ventricular surface.

(**C**) Proportion of $Ki67^+BrdU^+$ in all $BrdU^+$ cells and neuronal differentiation measured as $TUJ1^+/DAPI^+$ area. Data are expressed as mean ± standard deviation of the mean; n≥3 for each genotype and time point; ns, not significant $p \geq 0.05$, * $p < 0.05$, ** $p < 0.01$.

Figure 1

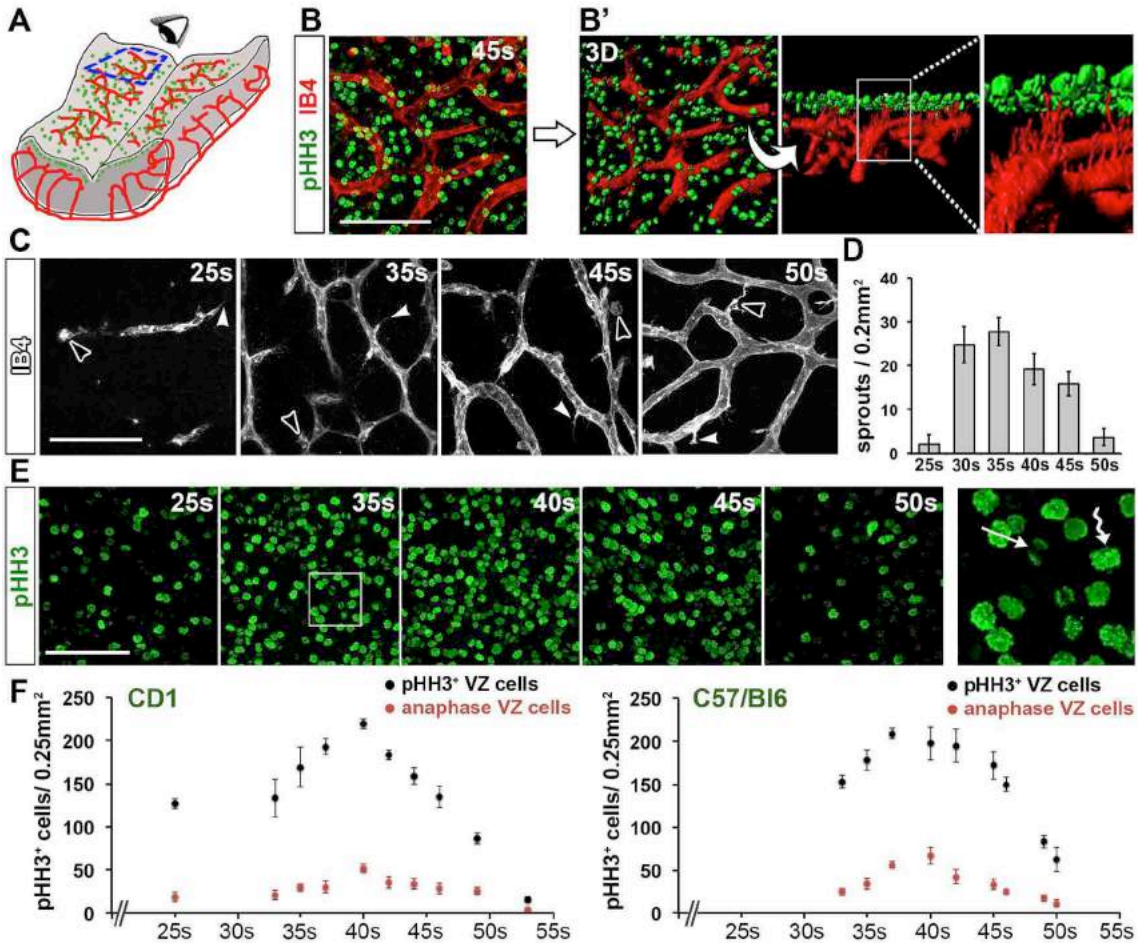
A
B
pHH3 IB4
45s
B'
3D
C
IB4
25s
35s
45s
50s
D
sprouts / 0.2mm²
25s 30s 35s 40s 45s 50s
E
pHH3
25s
35s
40s
45s
50s
F
CD1
pHH3⁺ VZ cells
anaphase VZ cells
pHH3⁺ cells/ 0.25mm²
25s 30s 35s 40s 45s 50s 55s
C57/Bl6
pHH3⁺ VZ cells
anaphase VZ cells
pHH3⁺ cells/ 0.25mm²
25s 30s 35s 40s 45s 50s 55s

Figure 2

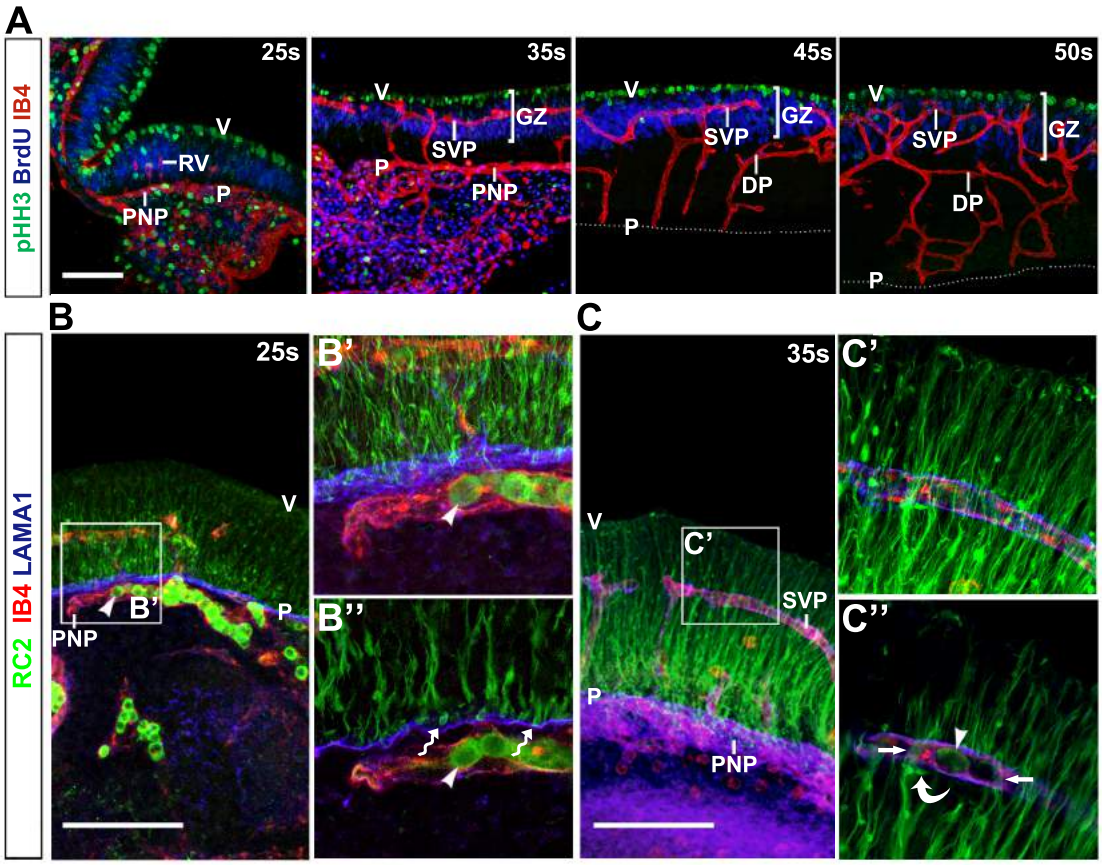
A
pHH3 BrdU IB4
25s
35s
45s
50s
V
RV
P
PNP
GZ
SVP
DP
B
B'
B''
C
C'
C''
RC2 IB4 LAMA1

Figure 3

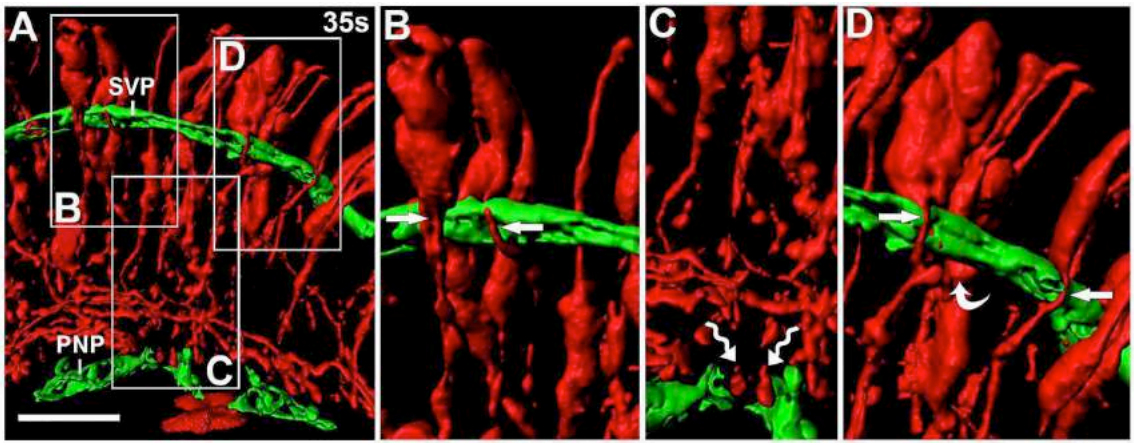

Figure 4

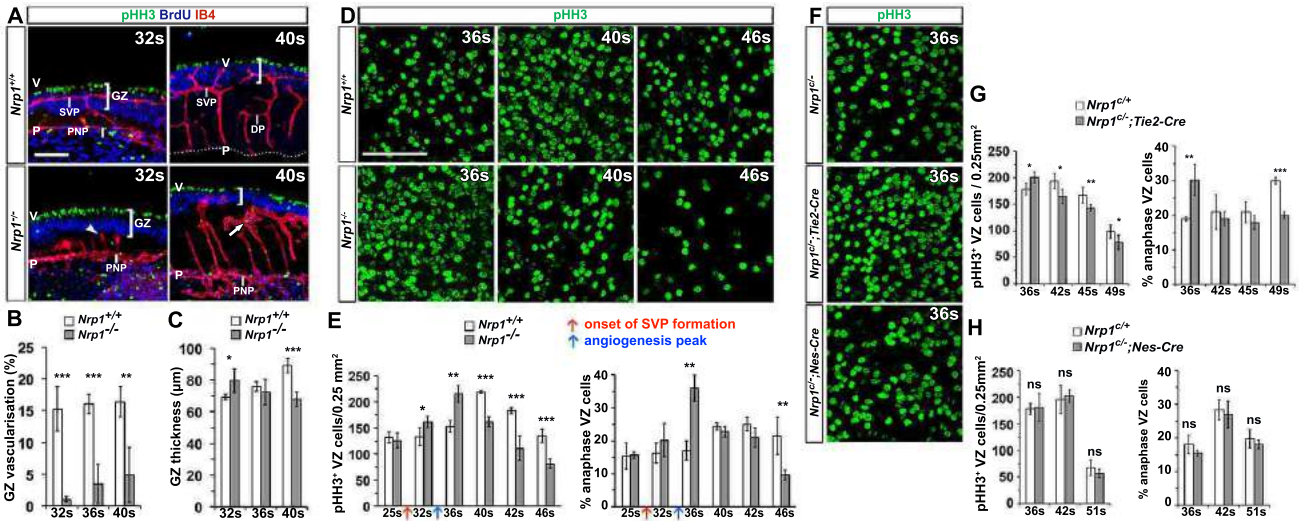
A
pHH3 BrdU IB4
32s
40s
Nrp1+/+
Nrp1-/-
V
GZ
SVP
P
PNP
DP
B
GZ vascularisation (%)
C
GZ thickness (µm)
D
pHH3
36s
40s
46s
E
pHH3+ VZ cells/0.25 mm2
% anaphase VZ cells
onset of SVP formation
angiogenesis peak
F
pHH3
Nrp1c/-
Nrp1c/-;Tie2-Cre
Nrp1c/-;Nes-Cre
G
Nrp1c/+
Nrp1c/-;Tie2-Cre
pHH3+ VZ cells / 0.25mm2
% anaphase VZ cells
H
Nrp1c/+
Nrp1c/-;Nes-Cre
pHH3+ VZ cells/0.25mm2
% anaphase VZ cells
ns

Figure 5

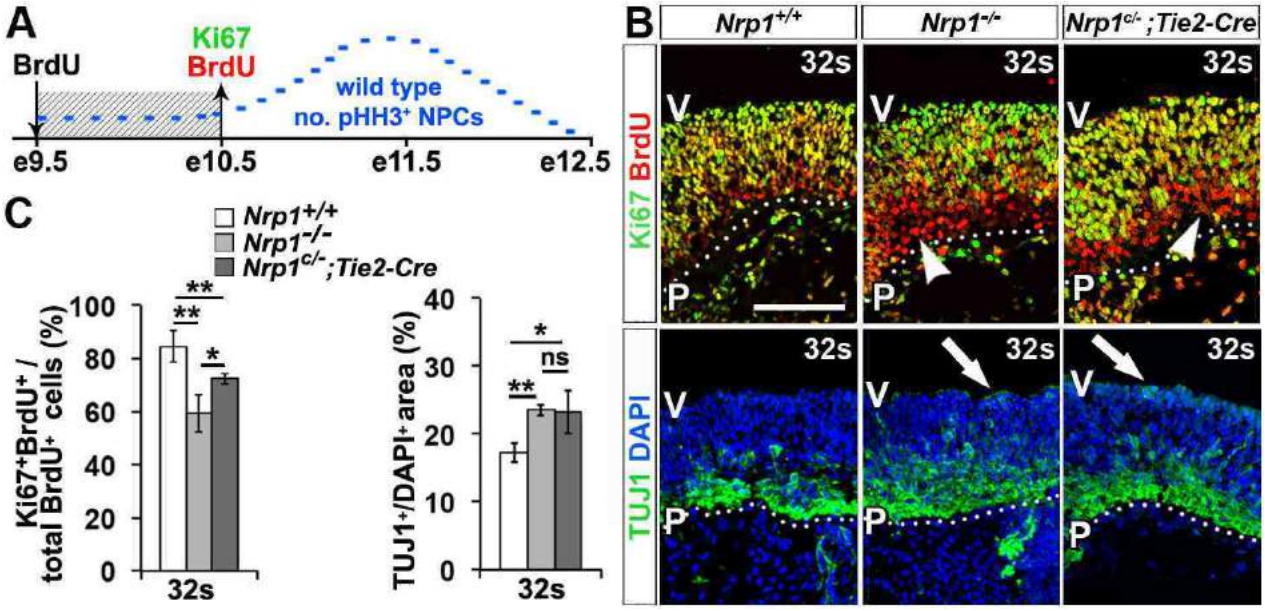
A
BrdU
Ki67
BrdU
wild type
no. pHH3+ NPCs
e9.5
e10.5
e11.5
e12.5
B
Nrp1+/+
Nrp1-/-
Nrp1c/-;Tie2-Cre
Ki67 BrdU
TUJ1 DAPI
32s
V
P
C
Nrp1+/+
Nrp1-/-
Nrp1c/-;Tie2-Cre
Ki67+BrdU+ / total BrdU+ cells (%)
TUJ1+/DAPI+ area (%)
32s
**
*
ns

Supporting information

Inventory or Supporting information:

Supplementary Materials and Methods

Supplemental References

Supplementary Tables

Supplementary Figure Legends

Supplementary Figures

Supplementary Materials and Methods

Animals. Animal work was carried out following UK Home Office and local ethical guidelines. To obtain embryos of defined developmental stages, mice were paired overnight and the day of finding a copulation plug was designated embryonic day (e) 0.5. To stage-match embryos within a litter and between litters, we compared the number of somite pairs (**Supplemental Table 1**). CD1 and C57BL/6 mice were obtained from Charles River Laboratories, UK. *Nrp1*-null mice on a CD1 background (1) and conditional endothelial- and NPC-specific NRP1-null mice on a C57/Bl6 background have been described previously (2). In some experiments, pregnant females were injected intraperitoneally with 10 mg/kg BrdU either 1 or 24 h before embryos were removed. *Sox1-iCreER^{T2}*mice were generated by pronuclear injection of a modified 197 kb mouse genomic PAC clone (RPCI21 502 P07) spanning 94 kb upstream and 103 kb downstream of *Sox1* and in which the *Sox1* open reading frame was replaced with an iCreER^{T2}-SV40-polyA cassette (3) using a previously published method (4). For mosaic labelling of hindbrain NPCs, pregnant *Rosa^{tdTomato}* females, following mating to *Sox1-iCreER^{T2}* males, received 20 mg/kg tamoxifen diluted in peanut oil by oral gavage 24 h before embryos were removed.

Fluorescence staining and imaging. Hindbrains were fixed for 2 h in 4% formaldehyde in PBS. In some experiments, hindbrains were embedded in 3% agarose and sectioned using a vibratome (70 μm) or embedded in OCT (Agar Scientific) and sectioned on a cryostat (10 μm). Hindbrains, floating sections and cryosections were incubated for 1 h at 4ºC in PBS containing 0.1% Triton X-100 (PBT) and 10% serum-free block (DAKO). Samples were incubated with primary antibodies in PBT at 4ºC overnight, washed in PBT and incubated in secondary antibodies in PBT at room temperature (RT) in the dark for 2 h. Labelled samples were counterstained with DAPI for 1 min, postfixed in 4% formaldehyde for 20 min and mounted on glass slides using SlowFade (Life Technologies) or Mowiol (Sigma). For BrdU staining, samples were incubated for 10 min each in 1N HCl at RT, followed by 2N HCl at RT and then 2N HCl at 37ºC. Samples were neutralised by washing twice in 0.1 M sodium tetraborate and three times in PBT for 5 min each. The following antibodies were used: rabbit α-phospho-histone H3 (pHH3; 1:400, Millipore, cat. no. 06-570), rat anti-BrdU (1:250, Abcam, cat no. ab6326), mouse anti-RC2 (1:10, Developmental Studies Hybridoma Bank, DSHB), rabbit anti-LAMA1 (1:30, Sigma, cat. no. L9393), rabbit anti-red fluorescent protein (RFP; 1:500, MBL, cat. no. PM005), rabbit anti-cleaved caspase 3 (1:200, Cell Signalling, cat. no. 9661), rabbit TUJ1 (1:250, BioLegend, cat. no. PRB-435), mouse anti-Ki67 (1:100, BD Pharmingen, cat. no. 550609) and rabbit anti-GLUT1 (1:200, Millipore, cat. no. 07-1401). We used AlexaFluor-conjugated secondary antibodies appropriate for the species of the primary antibody (1:200; Thermo Fisher). For blood vessel staining, we used biotinylated IB4

(1:200, Sigma) followed by AlexaFluor-conjugated streptavidin (1:200, Thermo Fisher). Labelled samples were imaged with an LSM710 confocal microscope (Zeiss, Jena) and processed with Photoshop CS6 (Adobe, Inc.). 3D reconstructions of z-stacks were performed with Imaris (Bitplane).

Quantification of immunolabelling. Quantification of phenotypes in confocal z-scans was performed with the count tool in Photoshop CS6. The number of $pHH3^+$ NPCs and $IB4^+$ endothelial tip cells was determined in two representative areas of 0.25 and 0.2 mm^2, respectively, in the anterior portion of each hindbrain hemisegment, and the 4 readings were averaged to obtain the value for that hindbrain. The number of $Ki67^+$ NPCs, $BrdU^+$ NPCs, ratio of $Ki67^+/BrdU^+$ NPCs and the area of TUJ1 labelling were determined in 3 cryosections (10 μm) for each hindbrain, and the 3 readings for each embryo were averaged to obtain the value for that hindbrain. Quantification of cleaved caspase 3^+ cells was performed similarly, but using 5 sections per hindbrain due to the overall low number of apoptotic cells at the developmental stages examined. To quantify the level of GLUT1 staining in the neural parenchyme, the pixel area of GLUT1 staining that was also positive for IB4 was subtracted from the pixel area of total GLUT1 staining to exclude the endothelial contribution to GLUT1 staining; the resulting value was then normalised to the overall area of the hindbrain cross-section. GLUT1 staining was determined in 3 cryosections for each hindbrain. Data shown in each graph are the average of 3 or more hindbrains per genotype and time point (see **Supplemental Table 2** for a complete list of the number of embryos analysed).

RNA extraction and qRT-PCR. Hindbrains were dissected from e10.5 embryos and total RNA was isolated using the RNeasy Micro Kit (Qiagen). cDNA was synthesised from isolated RNA by reverse transcription using Superscript IV (Thermo Fisher). qRT-PCR was performed with 50 ng cDNA on an ABI 7500 Fast Real-Time PCR System (Applied Biosystems) using SYBR Green PCR Master Mix (Applied Biosystems) and 0.45 μg of the following oligonucleotide pairs (Sigma-Aldrich): *Hif1a* 5'-AAACCACCCATGACGTGCTT-3' and 5'-GAGCGGCCCAAAAGTTCTTC-3', amplicon 182 bp; *Vegfa* 5'-CAGATCATGCGGATCAA-3' and 5'-TTGTTCTGTCTTTCTTTG-3', amplicon 100 bp; *Actb* 5'-AAGGCCAACCGTGAAAAGAT-3' and 5'-GTGGTACGACCAGAGGCATAC-3', amplicon 110 bp. For each gene, every sample was analysed in triplicate, and a no-template control was also included for each oligonucleotide pair. Data were collected using Sequence Detector Software (SDS version 2.2; Applied Biosystems), and expression levels were extrapolated using DART-PCR software (5) after normalisation to *Actb* expression levels.

Statistical analysis. To determine whether two datasets were significantly different, we determined

the *P* value with a two-tailed, unpaired *t* test using Excel (Microsoft). Statistical significance is reported in the figures (ns, $p \geq 0.05$; * $p < 0.05$; ** $p < 0.01$; *** $p < 0.001$).

Supplemental References

1. Kawasaki T, *et al*. (1999) A requirement for neuropilin-1 in embryonic vessel formation. *Development* 126(21):4895-4902.
2. Fantin A, *et al*. (2013) NRP1 acts cell autonomously in endothelium to promote tip cell function during sprouting angiogenesis. *Blood* 121(12):2352-2362.
3. Claxton S, *et al*. (2008) Efficient, inducible Cre-recombinase activation in vascular endothelium. *Genesis* 46(2):74-80.
4. Lee EC, *et al*. (2001) A highly efficient Escherichia coli-based chromosome engineering system adapted for recombinogenic targeting and subcloning of BAC DNA. *Genomics* 73(1):56-65.
5. Peirson SN, *et al*. (2003) Experimental validation of novel and conventional approaches to quantitative real-time PCR data analysis. *Nucleic Acids Res* 31(14):e73.

Supplementary Tables

Supplementary Table 1: Stage matching of mouse embryos. Embryos were stage matched by comparing the number of their somite pairs. The corresponding embryonic day post-conception (E) and average number of somite pairs (s) are shown for wildtype CD1 and C57Bl/6 mice.

Wildtype embryonic day (dpc)	9.5	10.5	11.5	12.5
Average number of somite pairs (s)	25	35	45	50

Supplementary Table 2: Sample sizes.

Number of embryos of the indicated genotypes analysed for each experiment.

Figure	Genotype	Developmental stage (sample size)
4B	*Nrp1*$^{+/+}$	32s (6), 36s (3), 40s (4)
	Nrp1$^{-/-}$	32s (4), 36s (4) 40s (5)
4C	*Nrp1*$^{+/+}$	32s (4), 36s (3), 40s (4)
	Nrp1$^{-/-}$	32s (3), 36s (4), 40s (5)
4E	*Nrp1*$^{+/+}$	25s (4), 32s (3), 36s (3), 40s (3), 42s (3) 46s (5)
	Nrp1$^{-/-}$	25s (3), 32s (6), 36s (3), 40s (4), 42s (6), 46s (3)
4G	*Nrp1*$^{c/+}$	36s (3), 42s (5), 45s (6), 49s (3)
	Nrp1$^{c/-}$ *Tie2-Cre*	36s (5), 42s (3), 45s (7), 49s (7)
4H	*Nrp1*$^{c/+}$	36s (3), 42s (6), 51s (3)
	Nrp1$^{c/-}$ *Nes-Cre*	36s (3), 42s (4), 51s (3)
5C	*Nrp1*$^{+/+}$	32s (3)
	Nrp1$^{-/-}$	32s (3)
	Nrp1$^{c/-}$ *Tie2-Cre*	32s (4)
S3	*Nrp1*$^{+/+}$	32s (3), 40s (4)
	Nrp1$^{-/-}$	32s (3), 40s (3)
S5	*Nrp1*$^{+/+}$	36s (3)
	Nrp1$^{-/-}$	36s (3)
S8	*Nrp1*$^{+/+}$	46s (3)
	Nrp1$^{-/-}$	46s (3)
S9A	*Nrp1*$^{+/+}$	32s (4)
	Nrp1$^{-/-}$	32s (3)
S9D	*Nrp1*$^{+/+}$ 20% O_2	32s (3)
	Nrp1$^{-/-}$ 20% O_2	32s (3)
	Nrp1$^{-/-}$ 80% O_2	32s (3)

Supplementary Figures and Figure legends

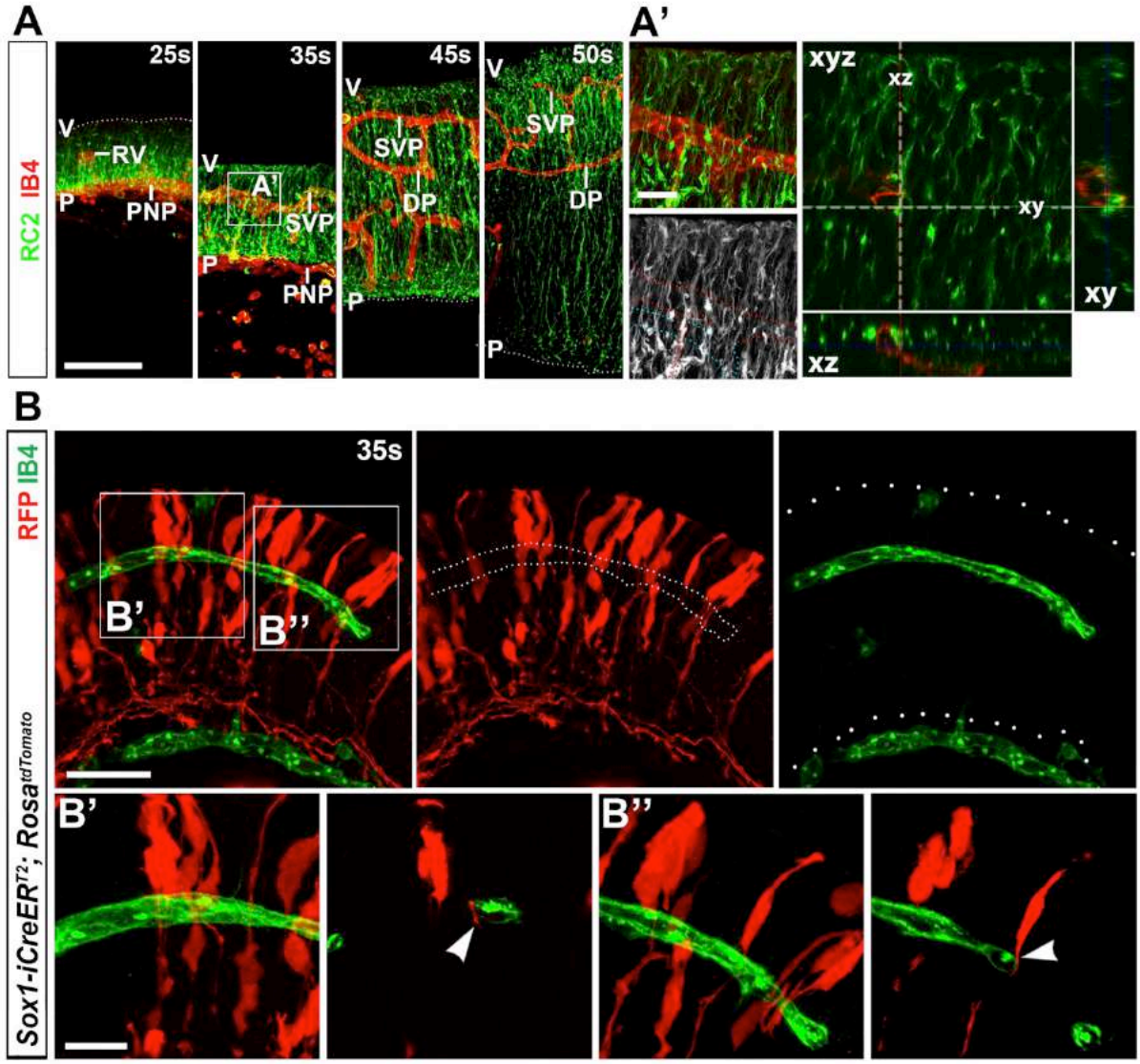

Supplementary Figure 1: NPC processes contact hindbrain vasculature.

(**A**) Maximal projections (xy) of confocal z stacks of 70µm transverse wildtype hindbrain sections at the indicated stages, labelled with IB4 for blood vessels and antibodies for the radial glia marker RC2. Scale bar: 100 µm. The boxed area in (**A**) is shown at higher magnification in (**A'**), with RC2 labelling only shown in grey scale in the lower left panel; outlines indicate position of blood vessel. Single (1.25 µm) optical section of the z stack shown in right panel. Flanking boxes display orthogonal xy and xz projections of single optical section; note how RC2^{+} densities directly contact IB4^{+} vessels. Scale bar: 20 µm.

(**B**) Maximal projections (xy) of confocal z stacks of a 70µm transverse sections of a *Sox1-iCreER^{T2};Rosa^{tdTomato}* 35s hindbrain after induction with 20mg/kg of tamoxifen for 24 hours, labelled with IB4 and antibodies for RFP to detect the tomato reporter. Dotted lines in the middle panel demarcate position of an SVP vessel, dotted lines in the right-hand panel demarcate the hindbrain surfaces. The boxed areas in (**B**) are shown at higher magnification in (**B, B''**), as a confocal z-stack (left panel) or single (1.25µm) optical section of each z stack (right panel). Arrowheads indicate RFP^{+} NPC processes contacting an SVP vessel. Scale bar: 50 µm (**B**), 20 µm (**B', B''**).

Abbreviations: P, pial surface; V, ventricular surface; RV, radial vessels; SVP, subventricular vascular plexus; DP, deep plexus; PNP, perineural vascular plexus; GZ, germinal zone.

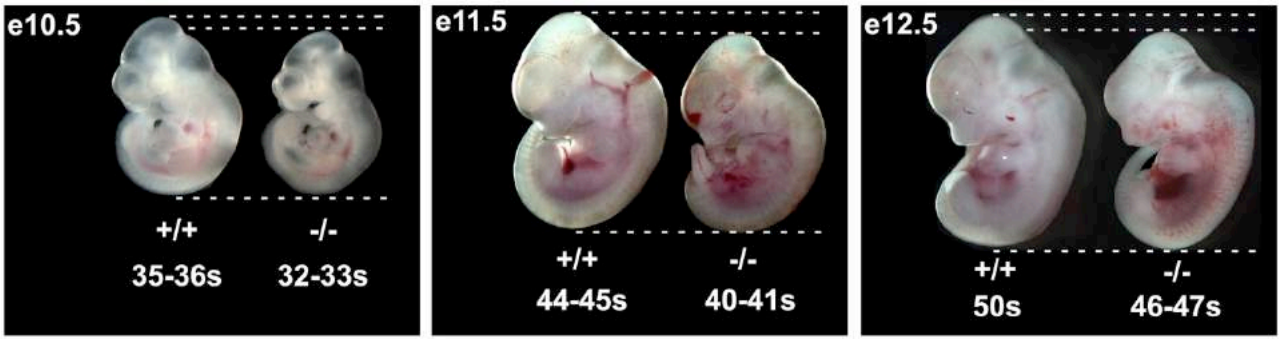

Supplementary Figure 2: *Nrp1*$^{-/-}$ embryos are developmentally delayed.
Representative brightfield images of wildtype (*Nrp1*$^{+/+}$) and *Nrp1*$^{-/-}$ littermates in the CD1 background at the indicated ages. The typical range of somite pairs at that age is shown for each genotype below the image of the embryo. Dotted lines highlight the reduced crown-rump length of mutants.

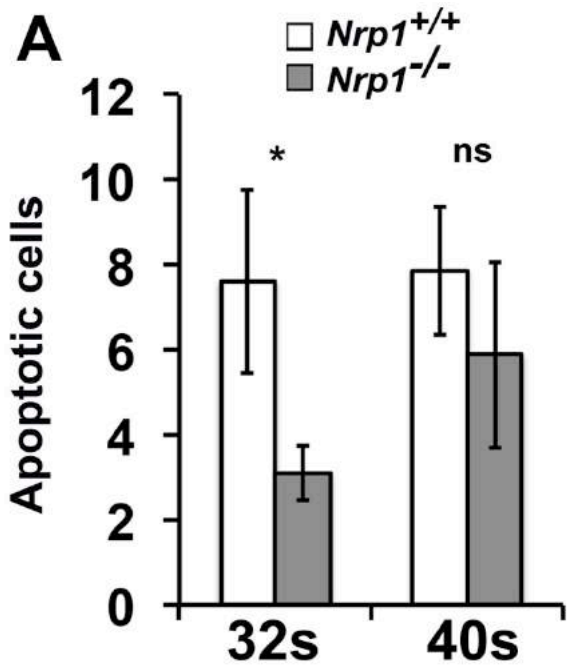

Supplementary Figure 3: Cell survival is not compromised in *Nrp1*$^{-/-}$ hindbrains.
Quantification of apoptotic (cleaved caspase 3^{+}) cells per 10 μm transverse hindbrain section at 32s and 40s. Data are the mean ± standard deviation of the mean; n≥3 for each genotype; ns, not significant, p≥0.05, * p<0.05.

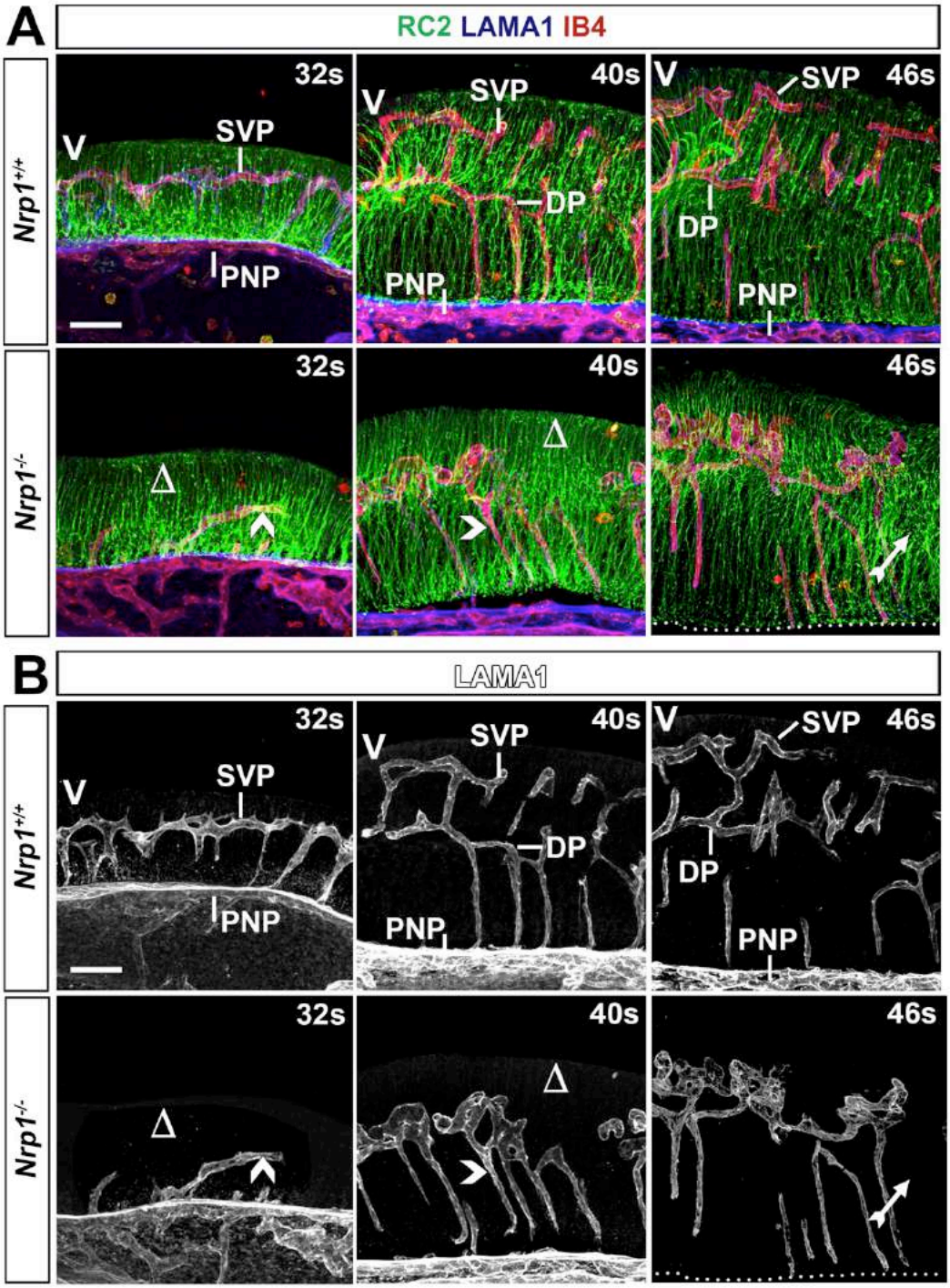

Supplementary Figure 4:

RC2^{+} processes and laminin expression in NRP1-deficient hindbrains.

(**A**) Maximal projections (xy) of confocal z stacks of 70μm transverse sections from stage-matched wildtype and *Nrp1*$^{-/-}$ hindbrains after labelling with IB4 and antibodies for RC2 (NPC processes) and LAMA1 (extracellular matrix).

(**B**) LAMA1 staining is preserved in the vasculature of NRP1-deficient hindbrains. **Δ** denotes avascular regions; chevrons indicate abnormally orientated vessels; the fletched arrow indicates a region of NPC process disorganisation.

Abbreviations: P, pial surface; V, ventricular surface; SVP, subventricular vascular plexus; DP, deep plexus; PNP, perineural vascular plexus; GZ, germinal zone. Scale bar: 100μm.

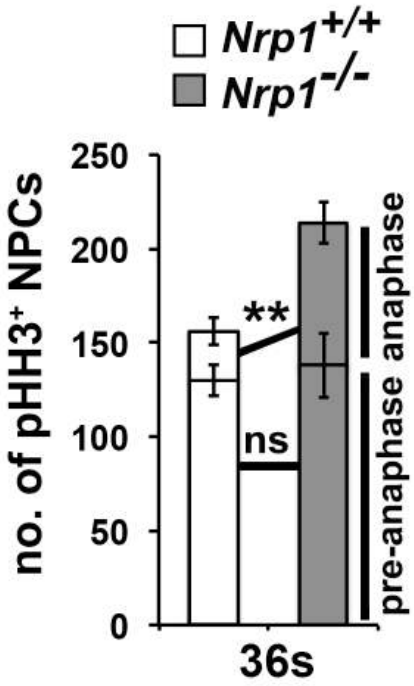

Supplementary Figure 5:

A significant proportion of NPCs stalls in anaphase in 36s *Nrp1*$^{-/-}$ hindbrains.

Quantification of the density of pre-anaphase and anaphase mitotic NPCs in stage-matched control and *Nrp1*$^{-/-}$ hindbrains at 36s, determined by wholemount pHH3 immunolabelling of the hindbrain VZ (see far-right panel in **Fig. 1E**). Data are expressed as mean ± standard deviation of the mean; n≥3 for each genotype; ns, not significant $p \geq 0.05$, ** $p < 0.01$.

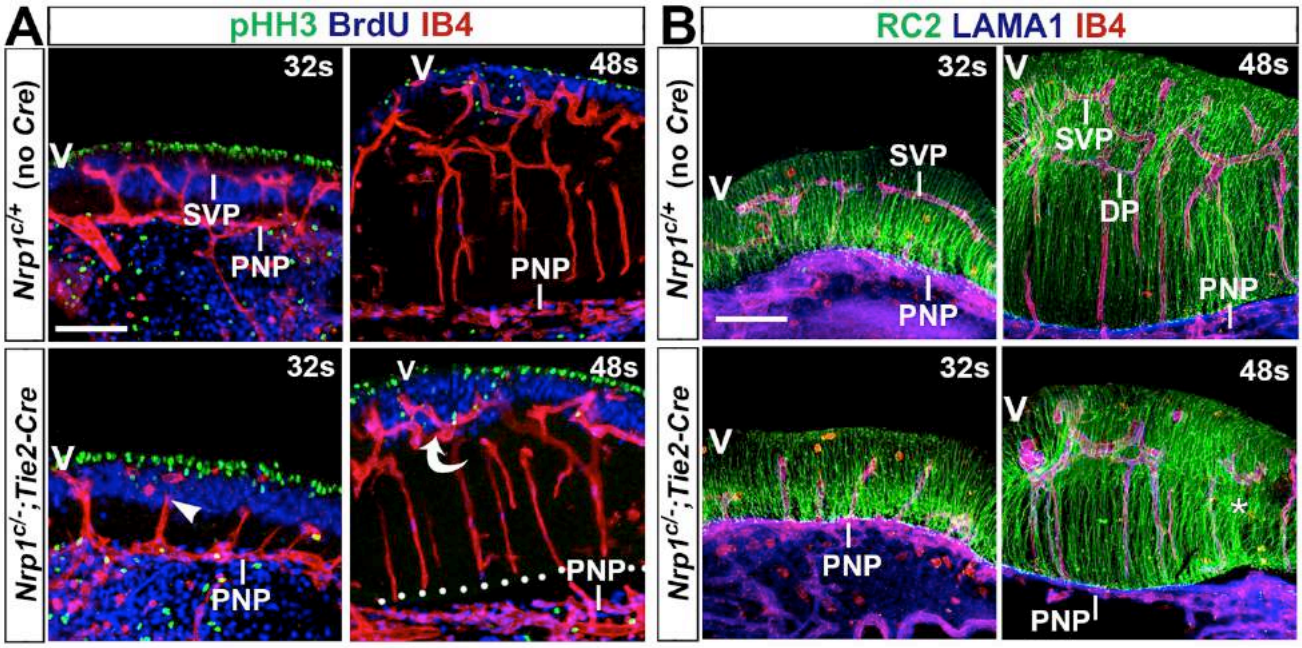

Supplementary Figure 6:

Endothelial NRP1 loss impairs hindbrain vascularisation, but not RC2 organisation.

Maximal projections (xy) of confocal z stacks of 70µm transverse sections of stage-matched control and *Tie2-Cre;Nrp1*$^{c/-}$ hindbrains at the indicated stages after labelling with IB4 and antibodies for pHH3 and BrdU (**A**) or antibodies for RC2 and LAMA1 (**B**). Arrowhead in (**A**) indicates blind-ended radial vessel; the asterisk in (**B**) indicates a region where NPC processes appear disorganised. The dotted line in (**A**) demarcates the pial hindbrain boundary at 48s; separation of the hindbrain parenchyme from the PNP in the perineural membrane is a sectioning artefact. Abbreviations: P, pial surface; V, ventricular surface; SVP, subventricular vascular plexus; DP, deep plexus; PNP, perineural vascular plexus. Scale bar: 100 µm.

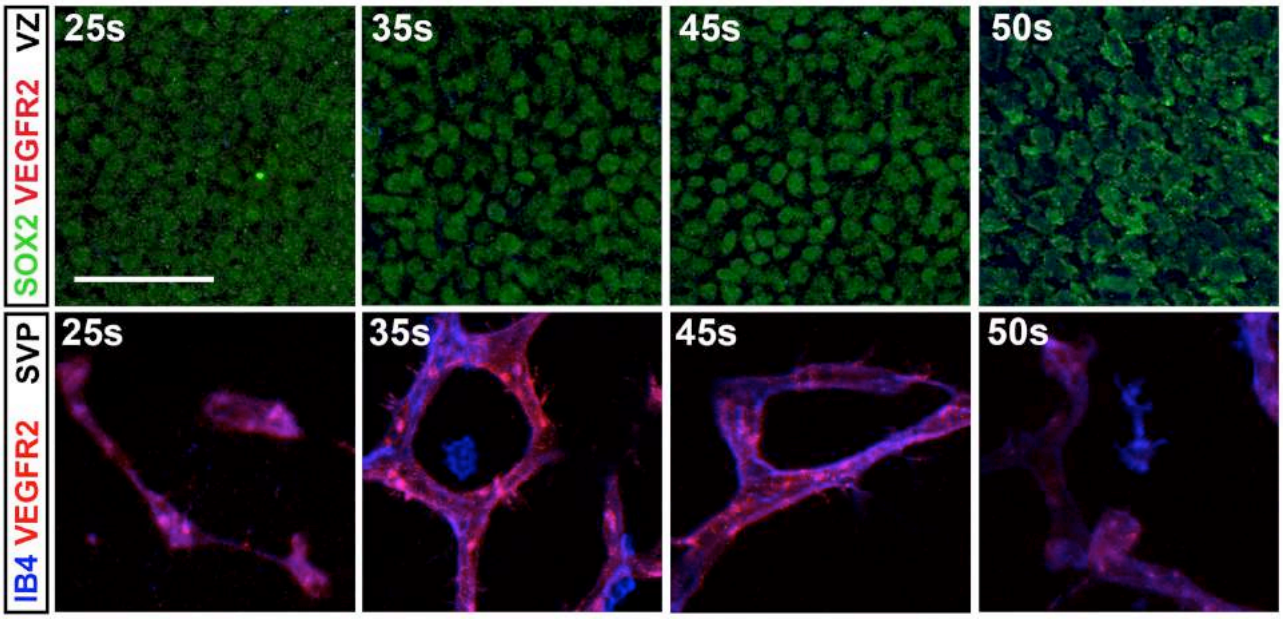

Supplementary Figure 7: VEGFR2 is expressed by vessels, but not NPCs in the hindbrain.

Maximal projection (xy) of confocal z stacks of mouse embryo hindbrains at the indicated stages after labelling with the dual vessel and microglia marker IB4 together with antibodies for SOX2 to detect NPC nuclei. Flatmounted hindbrains were, imaged at the level of the VZ (top panels) or SVP (bottom panels) for each hindbrain and at each stage. Abbreviations: VZ, ventricular zone; SVP, subventricular vascular plexus. Scale bar: 100μm.

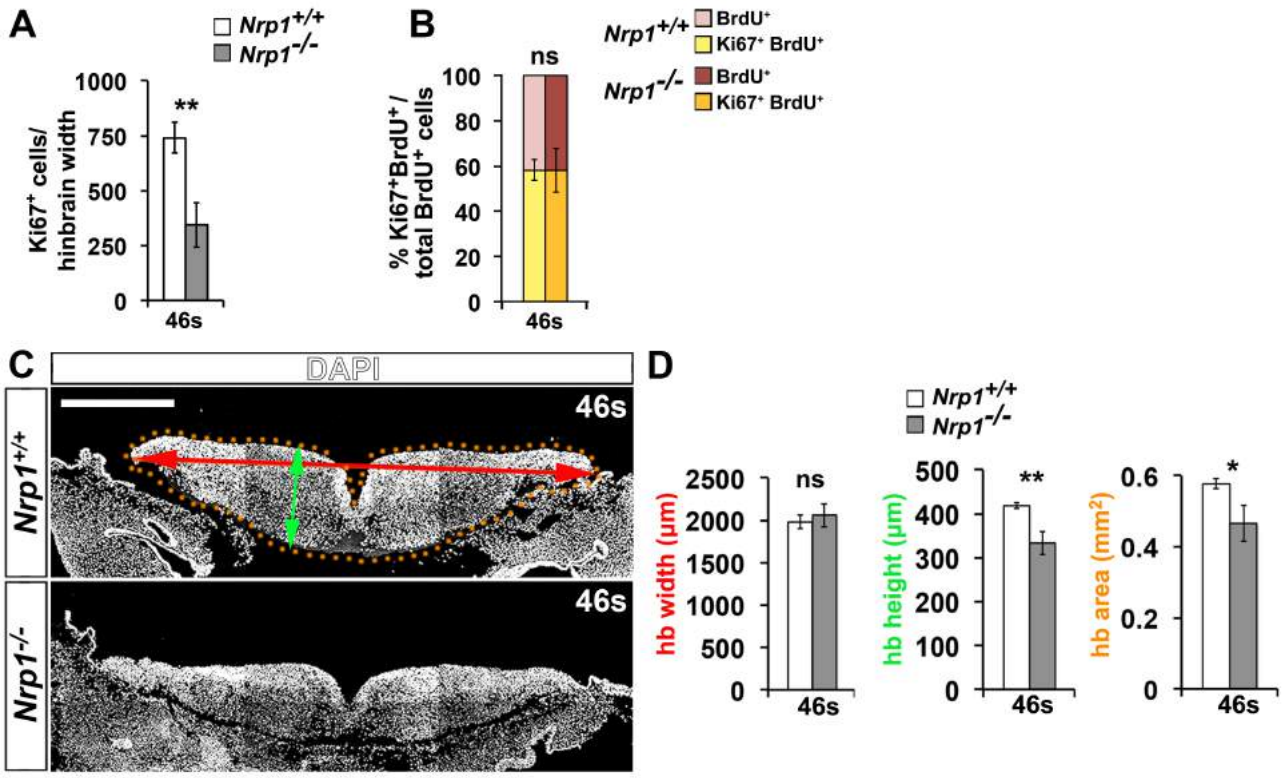

Supplementary Figure 8: Loss of hindbrain NPCs correlates with stunted hindbrain growth.

(**A,B**) NRP1-deficient hindbrains contain fewer cycling NPCs at 46s. Quantification of the total number of Ki67^{+} cells per section (**A**) and proportion of Ki67^{+}BrdU^{+} in all BrdU^{+} cells (**B**) in 46s control and *Nrp1*$^{-/-}$ hindbrains. For this analysis, embryos were injected with BrdU and analysed hindbrains 24 h later. Data are expressed as mean ± standard deviation of the mean; n=3 embryos for each genotype; ** $p<0.01$; ns, not significant $p\geq0.05$.

(**C,D**) Reduced growth of *Nrp1*-null hindbrains. Maximal projections of confocal tile scan z stacks of 10 µm transverse sections through 46s wildtype and *Nrp1*-null DAPI-stained hindbrains (**C**) including arrows to illustrate measurements taken to determine hindbrain lateral width (red line), radial height (green line) and cross-sectional area (orange dotted outline). (**D**) Quantification of lateral width, radial height and area of hindbrain (hb), expressed as mean ± standard deviation of the mean; n=3 for each genotype; ns, not significant, $p\geq0.05$, * $p<0.05$, ** $p<0.01$. Scale bar: 100µm.

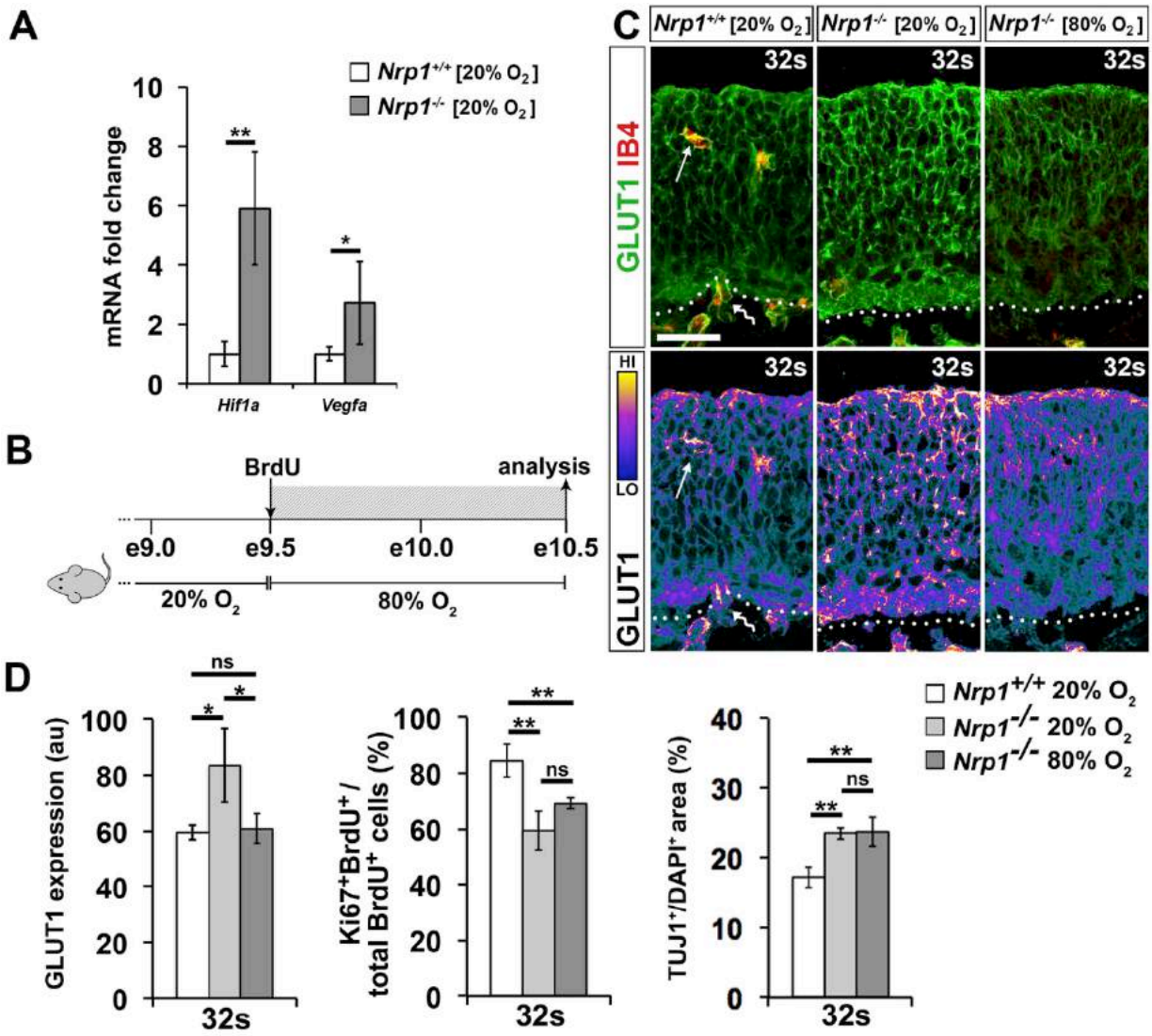

Supplementary Figure 9: The SVP does not regulate NPCs by relieving tissue hypoxia.

(**A**) Increased expression of the hypoxia-regulated genes *Hif1a* and *Vegfa* in 32s *Nrp1*-null hindbrains. Expression levels were determined by qPCR analysis, normalised to *Actb* and expressed as fold change compared to stage-matched wildtype hindbrains. Data are expressed as mean ± standard deviation of the mean, n≥3 for both genotypes; * p<0.05, ** p<0.01.

(**B-D**) Rescue of hindbrain hypoxia, but not NPC self-renewal defects, in 32s *Nrp1*-null hindbrains by housing pregnant dams in a hyperoxic atmosphere. (**B**) Schematic representation of the hypoxia rescue experiment. Pregnant dams received an intraperitoneal BrdU injection when their embryos where at e9.5 and were then transferred from normoxia to an 80% oxygen atmosphere for 24 hours before analysis e10.5. (**C**) 10 µm transverse sections from hindbrains of 32s wildtype and *Nrp1*$^{-/-}$ embryos from dams housed in 20% oxygen and *Nrp1*-null embryos from dams in an 80% oxygen environment, labelled for GLUT1 (green) and IB4 (red). 'Heatmap' for GLUT1 staining shown in lower panels. Scale bar: 25 µm. Arrows and wavy arrows indicate the GLUT1^{+} SVP and PNP, respectively. (**D**) Hyperoxia rescues oxygenation of *Nrp1*-null hindbrains (left-hand graph; arbitrary units, au). NPC self-renewal (percentage of Ki67^{+}BrdU^{+} double-labelled NPCs) and neuronal differentiation (TUJ1^{+} hindbrain area), shown in middle and right-hand graphs, respectively). Data are expressed as mean ± standard deviation of the mean; n=3 for each genotype and oxygen level; ns, not significant, p≥0.05, * p<0.05, ** p<0.01.